CHINESE OPTICS LETTERS

Vol. 19, No. 12 | December 2021

Uncertainty evaluation of the second-order Zeeman shift of a transportable ^{87}Rb atomic fountain clock

Henan Cheng (程鹤楠)[1,2], Siminda Deng (邓思敏达)[1,2], Zhen Zhang (张 镇)[1,2], Jingfeng Xiang (项静峰)[1], Jingwei Ji (吉经纬)[1], Wei Ren (任 伟)[1], Tang Li (李 唐)[1], Qiuzhi Qu (屈求智)[1], Liang Liu (刘 亮)[1*], and Desheng Lü (吕德胜)[1,2**]

[1] Key Laboratory of Quantum Optics, Shanghai Institute of Optics and Fine Mechanics, Chinese Academy of Sciences, Shanghai 201800, China

[2] College of Materials Science and Opto-Electronic Technology, University of Chinese Academy of Sciences, Beijing 100049, China

*Corresponding author: liang.liu@siom.ac.cn

**Corresponding author: dslv@siom.ac.cn

Received March 24, 2021 | Accepted May 14, 2021 | Posted Online September 1, 2021

In this article, taking advantage of the special magnetic shieldings and the optimal coil design of a transportable Rb atomic fountain clock, the intensity distribution in space and the fluctuations with time of the quantization magnetic field in the Ramsey region were measured using the atomic magneton-sensitive transition method. In an approximately 310 mm long Ramsey region, a peak-to-peak magnetic field intensity of a 0.74 nT deviation in space and a 0.06 nT fluctuation with time were obtained. These results correspond to a second-order Zeeman frequency shift of approximately $(2095.5 \pm 5.1) \times 10^{-17}$. This is an essential step in advancing the total frequency uncertainty of the fountain clock to the order of 10^{-17}.

Keywords: Zeeman effect; hyperfine structure; atomic clock; magnetic-sensitive method.

DOI: 10.3788/COL202119.120201

1. Introduction

Over past decades, atomic fountain clocks have been utilized widely as a stable frequency standard in metrology[1–6]. Cs fountain clocks have greatly improved the accuracy and stability of the International System of Units (SI) second[7]. The ^{87}Rb fountain clock is more attractive for applications as a secondary representation of the SI second because the collision-induced fractional frequency shift of cold ^{87}Rb atoms is smaller than that of ^{133}Cs atoms[8,9]. Six highly stable and robust Rb fountains currently operate at two ground stations of the Global Positioning System in the United States Naval Observatory[10]. Presently, the frequency uncertainty of the most accurate fountain clocks in the world is approximately $(2–3) \times 10^{-16}$[11–13]. However, some studies suggested that the frequency uncertainty of fountain clocks can be improved to the order of 10^{-17}. Among several factors affecting the frequency uncertainty of fountain clocks, the second-order Zeeman effect caused by the interaction between the magnetic field and atoms is one of the most important items. To achieve a stable and accurate fountain clock, the influence of this item on the output frequency of the atomic clock must be dealt with carefully.

For a fountain clock, the frequency uncertainty evaluation of the effects on the second-order Zeeman comprises two main aspects, which are the spatial distribution and time fluctuation of the quantization magnetic field in the region of the Ramsey interaction between cold atoms and microwave. Once a fountain atomic clock is integrated, measuring the magnetic field directly is difficult because of the obstacles of the vacuum chamber walls, magnetic shielding, and other structures. Several methods are used to measure the magnetic field indirectly depending on the interaction between the atoms and the magnetic field. They are mainly as follows: (I) low-frequency transition method[14], (II) magneto-sensitive transition method[15–17], (III) microwave antenna radiation method[18], and (IV) stimulated Raman transition method[19,20]. Each of these methods has its advantages and disadvantages. The Ramsey magneto-sensitive transition method is a good trade-off considering the measurement accuracy and convenience. However, this method requires a high degree of spatial uniformity for the magnetic field to be measured because magnetic-induced broadening mechanisms affect the visibility of the Ramsey fringes[21].

This paper reports the magnetic field intensity measurement distribution in the cold atoms flight trajectory of a transportable fountain clock. The fountain clock frequency uncertainty caused by spatial inhomogeneity and temporal drift of the magnetic field was evaluated in terms of the magnetic field measurements.

2. Method of Second-Order Zeeman Shift Uncertainty Evaluation

In the presence of a weak external magnetic field, the split of the ^{87}Rb atoms ground state hyperfine energy levels can be described using the Breit–Rabi formula[22]:

$$(F, m_F) = -\frac{E_0}{2(2I+1)} + m_F \mu_B g_I B \pm \frac{E_0}{2}\left(1 + x^2 + \frac{4m_F x}{2I+1}\right)^{\frac{1}{2}},$$
$$x = \frac{(g_J - g_I)\mu_B B}{\Delta E_0}. \quad (1)$$

In this formula, E_0 is the energy of the unperturbed ground state energy level, $m_F = m_I \pm m_J = m_I \pm 1/2$ is the quantum number of the magneton energy level, $\mu_B = h \cdot 1.399624604\,\mathrm{MHz/G}$ is the Bohr magneton, and B is the magnitude of the external magnetic field.

Under a weak magnetic field for $x \le 1$, Eq. (1) can be approximated as

$$E(F, m_F) = -\frac{E_0}{2(2I+1)} + \frac{g_I}{g_J + g_I} m_F E_0 x \pm \frac{E_0}{2}\left\{1 + \frac{2m_F x}{2I+1} + \frac{x^2}{2}\left[1 - \frac{4m_F^2}{(2I+1)^2}\right]\right\}. \quad (2)$$

From Eq. (2), the energy-level differences with different F quantum numbers and magnetic quantum numbers can be expressed as

$$\Delta E_{F_1, m_F \to F_2, m_F'} = \frac{g_I}{g_J + g_I}(m_F - m_F')\Delta E_0 x \pm \frac{\Delta E_0}{2}\left\{2 + \frac{2(m_F + m_F')x}{2I+1} + x^2\left[1 - \frac{2(m_F^2 + m_F'^2)}{(2I+1)^2}\right]\right\}, \quad (3)$$

where ΔE_0 is the unperturbed clock transition energy-level difference, $\Delta E_0 = h\nu_0$; g_I and g_J are the g factors of the electron and the nucleus, which are $g_J = 2.00233113(20)$ and $g_I = -9.951414(10) \times 10^{-4}$ for ^{87}Rb[23].

For the clock transition, $F = 2$, $m_F = 0 \to F = 1$, $m_F = 0$,

$$\Delta E_{F=2, m_F=0 \to F=1, m_F=0} = \frac{\Delta E_0}{2}(2 + x^2). \quad (4)$$

Thus, the clock transition frequency under magnetic field perturbation can be written as

$$\nu' = \frac{\nu_0}{2}(2 + x^2) = \nu_0 + \frac{\nu_0}{2}x^2 = \nu_0 + 575.15 \times 10^8 \langle B^2 \rangle. \quad (5)$$

The first term in Eq. (5) is the intrinsic clock frequency, and the second term is the frequency shift due to the second-order Zeeman effect. The frequency shift caused by the first-order Zeeman effect is zero, which is one of the main reasons for choosing this transition as a clock transition.

$\langle\,\rangle$ represents the time-averaged value along the drift length. When the C-fields are inhomogeneous, $\langle B^2 \rangle$ is given by $\langle B^2 \rangle = \langle B \rangle^2 + \sigma^2$. σ^2 is the variance of the magnetic field B along the atomic trajectory.

For magneto-sensitive $F = 2, m_F = -1 \to F = 1, m_F = -1$,

$$\Delta\upsilon_{F=2, m_F=-1 \to F=1, m_F=-1} = \frac{\nu_0}{2}(2 - x) = \nu_0 - 1.4 \times 10^{10} \langle B \rangle. \quad (6)$$

Hence,

$$\frac{\Delta\upsilon_{F=2, m_F=0 \to F=1, m_F=0}}{\upsilon_0} = 2\left(\frac{\Delta\upsilon_{F=2, m_F=-1 \to F=1, m_F=-1}}{\upsilon_0}\right)^2. \quad (7)$$

For ^{87}Rb, it follows from Eqs. (3)–(5) and (7) that

$$\frac{\Delta\nu_{\text{second zeeman}}}{\nu_0} = 2\left(\frac{\Delta\nu_{(-1,-1)}}{\nu_0}\right)^2 + 575.15 \times 10^8 \frac{\sigma^2}{\upsilon_0}. \quad (8)$$

From the first term in Eq. (8), the uncertainty of the second-order Zeeman shift is dominated by the temporal instability of the magnetic field, which is given by the following:

$$\delta\left(\frac{\Delta\nu_{\text{second zeeman}}}{\nu_0}\right) = \delta\left[2\left(\frac{\Delta\nu_{(-1,-1)}}{\nu_0}\right)^2\right] = 4 \times \frac{\Delta\nu_{(-1,-1)}}{\nu_0^2} \times \delta(\Delta\nu_{(-1,-1)}), \quad (9)$$

where $\delta(\Delta\nu_{(-1,-1)})$ is the temporal fluctuation of $\nu_{(-1,-1)}$.

According to Eq. (8), the relative frequency shift of the second-order Zeeman can be obtained as soon as the central frequency of the $(-1, -1)$ transition is measured experimentally. Furthermore, an evaluation of the second-order Zeeman frequency shift uncertainty comprises two aspects. One is the second-order Zeeman shift uncertainty caused by the measurement error σ^2 of the central frequency position and the calculation error of the magnetic field, which can be obtained from the second term of Eq. (8). Additionally, there is uncertainty due to long temporal fluctuations in the magnetic field, which can be derived from Eq. (9). The frequency shift uncertainty can be reduced in two ways. The first method reduces the fluctuations in the magnetic field, which guarantees the stability of the power supply to the C-field current source. When the temporal instability of the magnetic field is lower than 0.2 nT, i.e., the central fringe fluctuates less than 2.8 Hz, the uncertainty is in the order of 10^{-16}. The second way involves reducing the detuning of the $(-1, -1)$ magneto-sensitive transition central fringe from the $(0, 0)$ transition central fringe. This means that the C-field current and the magnitude of the magnetic field in the flight region are reduced. Most fountain clocks in many laboratories have a C-field magnetic field of 100 nT and above, such that the detuning of the $(-1, -1)$ magneto-sensitive transition is approximately 1400 Hz and above. This provides an uncertainty of approximately 3.4×10^{-16} for magnetic field fluctuations of about 0.2 nT. In the work of this article, the magnetic field was set to approximately 50 nT so that the uncertainty is

approximately 1.7×10^{-16} for the same magnetic field fluctuations. The premise of reducing the intensity of the magnetic field is to ensure that there are no zero magnetic intensity field points in the trajectory of cold atoms after state selection. Otherwise, the Majorana transition will deteriorate the frequency stability of the atomic clock.

The uncertainty of the second-order Zeeman frequency shift can be reduced by appropriately reducing the intensity of the magnetic field and minimizing the fluctuations of the magnetic field with time. This also makes it possible to improve the uncertainty of the second-order Zeeman frequency shift to the order of 10^{-17}.

3. Magnetic-Sensitive Ramsey Interference Experiment

Figure 1(a) shows the experimental configuration: from top to bottom are the ion pump, the Ramsey interrogation zone, the detection zone, the state-selective zone, and the cooling zone. To provide a uniform vertical upward magnetic field in the Ramsey interaction zone and a free flight zone, the magnetic field coils were designed for the fountain clock, as shown in Fig. 1(b). Nine sets of magnetic field coils were distributed out of the vacuum chamber in the Ramsey interaction zone. One main coil generates a quantization constant magnetic field in the axial direction along the atomic flight trajectory. Four sets of top compensation coils and four sets of bottom compensation coils compensate for inhomogeneities in the magnetic field due to the ends and center of the Lorentz coil. In this manner, a uniform vertical upward magnetic field of approximately 50 nT is generated in the axis of the coil. On the exterior of the magnetic field coils, there are five layers of Permalloy magnetic shields. This magnetic shielding is used to suppress the influence of the environmental external magnetic field on the inner magnetic field of the fountain clock with a shielding factor of approximately 1.5×10^4. The first and second layers of the magnetic shield cover only the Ramsey interrogation zone, whereas the remaining three layers cover the entire body of the fountain. This can cause the magnetic field in the state-selective zone to be in the opposite direction of the Ramsey interrogation zone. Consequently, for the direction of the magnetic field to be coherent along the atomic flight path, a set of compensation coils was assembled in the area of the state-selective zone to the detection zone, which is in the same direction as the C-field magnetic field.

Based on the method for evaluating the second-order Zeeman frequency shift uncertainty of fountain clocks in Section 2, the spatial distribution of the magnetic field intensity in the free flight zone first needs to be measured. The Ramsey fringes of the magneto-sensitive transition can be obtained using the $|F=2,m_F=-1\rangle \rightarrow |F=1,m_F=-1\rangle$ magneto-sensitive transition by applying two $\pi/2$ pulses near the $|F=2,m_F=-1\rangle \rightarrow |F=1,m_F=-1\rangle$ resonant frequency to the cold atom cloud when it passes through the microwave cavity twice during its upthrow and descent. Figure 2 shows a graphical representation of two magneto-sensitive transitions from the cooling zone at 3.19 and 3.24 m/s, respectively, with the apex of the atomic group upthrown at a distance of 10 and 28 mm above the

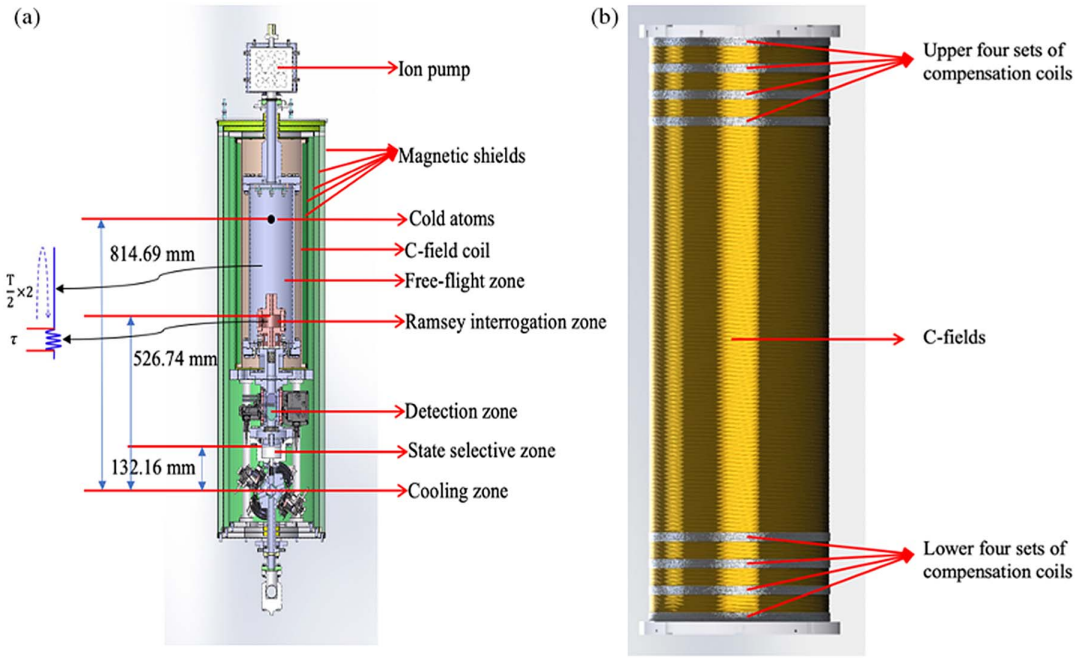

Fig. 1. (a) Schematic diagram of the experimental installation of the Rb fountain. There are five layers of magnetic shields to suppress the environmental magnetic field. The entire setup functions in a temperature-controlled cabinet. (b) C-field and eight sets of compensation coils. Solenoid coils and other auxiliary compensation coils construct the uniform magnetic field of the Ramsey interrogation zone and free flight zone. It has an average magnetic field of approximately 50 nT.

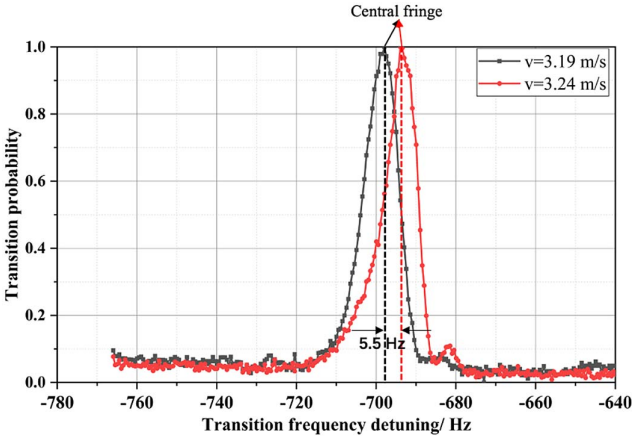

Fig. 2. Graphical representation of two magneto-sensitive transitions from the cooling zone at 3.19 and 3.24 m/s. Average magnetic field change of approximately 0.4 nT for a central fringe shift of approximately 5.5 Hz for the two magneto-sensitive transition fringes.

microwave cavity, respectively. This results in a broad transition spectrum and a high signal-to-noise ratio for the central transition fringe only because the time between the two upthrown velocity groups and the microwave is very short. On the basis of the frequency difference between the central fringe of this spectrum and the $|F=2,m_F=0\rangle \rightarrow |F=1,m_F=0\rangle$ transition, average magnetic field intensities of 49.9 and 49.5 nT were inversed in the region of the free upward of the atomic group, respectively.

On the basis of the two Ramsey spectral lines shown above, the launched atoms cloud velocity was increased continuously so that the height of the upthrow was increased by 10 mm each time. The movement of the Ramsey central fringe and the formation of a new fringe were then observed. By measuring the position of the Ramsey central fringe for each ejection velocity, the magnetic field at a single point in the atomic flight trajectory was obtained using the deconvolution method. Figure 3 shows the Ramsey fringes for ejection velocities of 3.94, 3.97, and 4.00 m/s, respectively. The detuning of the Ramsey central fringe was −702.1, −702.1, and −702.9 Hz, respectively, and the average magnetic field in the atomic flight trajectory was calculated to be 50.15, 50.15, and 50.2 nT. As the atom passed through the inhomogeneous C-field twice in its trajectory, the position of the central Ramsey fringe was no longer the highest point of the Rabi pedestal, as shown in Fig. 3.

The magnetic field at a single point in the flight trajectory of the atom was obtained using the deconvolution method by measuring the position of the Ramsey central fringe in the flight trajectory. Figure 4 presents a time-averaged magnetic field map. When the fountain is operated with 4 m/s, the central fringe of the $|F=2,m_F=-1\rangle \rightarrow |F=1,m_F=-1\rangle$ magneto-sensitive transition is approximately 702.9 Hz relative to the $|F=2,m_F=0\rangle \rightarrow |F=1,m_F=0\rangle$ clock transition, and the magnetic field is calculated as 50.22 nT. The peak-to-peak variation of space magnetic field in the Ramsey region is about 0.74 nT. From Eq. (5), the second-order Zeeman frequency shift was

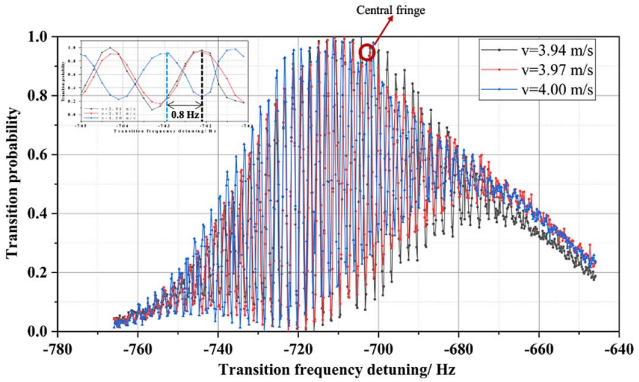

Fig. 3. Ramsey fringes for ejection velocities of 3.94, 3.97, and 4.00 m/s. The embedded image is an enlargement of Ramsey's central fringe. From the embedded diagram, the Ramsey central fringe shifts by approximately 0.8 Hz, which corresponds to an average magnetic field fluctuation of 0.05 nT.

calculated to be 2.1×10^{-14}. Consequently, the uncertainty of the second-order Zeeman frequency shift due to the spatial inhomogeneity of the magnetic field was 3.4×10^{-19} from the second term of Eq. (6), which is negligible compared with order of 10^{-17}.

The temporal instability of the magnetic field $\langle B\rangle$ has a major influence on the uncertainty of the second-order Zeeman frequency shift. The clock frequency uncertainty due to the temporal instability of the magnetic field can be obtained by monitoring the fluctuations of the magnetic field at a fixed position over a long time. The launched atoms cloud velocity was set to 4 m/s, corresponding an about 306 mm above the Ramsey cavity. The center Ramsey fringes of the $|F=2,m_F=-1\rangle \rightarrow |F=1,m_F=-1\rangle$ magneto-sensitive transition were obtained by sweeping 140 frequency points with a 0.05 Hz step. It took about three minutes to complete a frequency sweep. From Fig. 5,

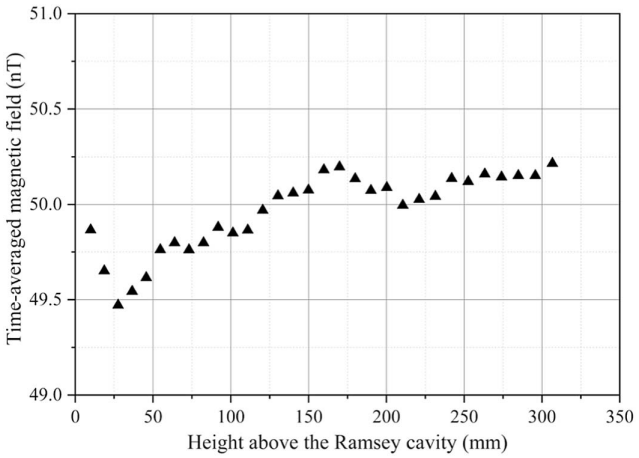

Fig. 4. Time-averaged magnetic field map. Measured position of the (−1, −1) magnetic-sensitive central Ramsey fringe as a function of the height above the Ramsey cavity. The origin of the horizontal axis corresponds to the center of the Ramsey cavity. The peak-to-peak variation of space magnetic field in Ramsey region is about 0.74 nT.

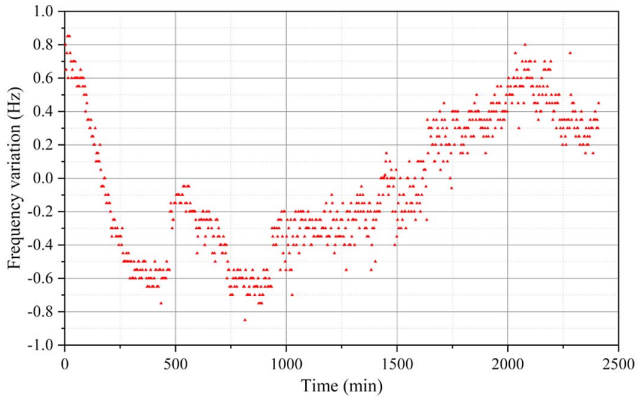

Fig. 5. Monitoring the central Ramsey fringe of the $|F = 2, m_F = -1\rangle \rightarrow |F = 1, m_F = -1\rangle$ transition for nearly 2 days. The temporal variation did not exceed ±0.85 Hz, which corresponds to a magnetic field variation of 0.06 nT.

the central Ramsey fringe transition frequency fluctuations were monitored for nearly 2 days. The temporal variation of the center Ramsey frequency did not exceed ±0.85 Hz. Thus, using Eq. (9), the calculated uncertainty due to the temporal instability of the magnetic field is about 5.1×10^{-17}.

Thus, the total uncertainty on the second-order Zeeman shift correction is 5.1×10^{-17}, and the typical correction is

$$\frac{\Delta\nu_{\text{second zeeman}}}{\nu_0} = (2095.5 \pm 5.1) \times 10^{-17}. \tag{10}$$

4. Conclusion

Ramsey fringes with different velocities were obtained using the magneto-sensitive transition method on the basis of a special design of magnetic shielding and magnetic field control parameters for a transportable Rb fountain. The second-order Zeeman frequency shift and the uncertainty of the Shanghai Institute of Optics and Fine Mechanics (SIOM) fountain clock were evaluated using the Ramsey fringes method. The second-order Zeeman frequency shift uncertainty was reduced by decreasing the size of the magnetic field across the C-field zone. The average magnetic field of the atom's flight trajectory was 49.96 ± 0.20 nT. Consequently, its second-order Zeeman frequency shift was 2.0955×10^{-14}, and its frequency uncertainty was 5.1×10^{-17}. This is an important step in advancing the total frequency uncertainty of the fountain clock to the order of 10–17.

Acknowledgement

We thank Dr. Rong Wei for his helpful proposal to improve the uniformity of the quantization magnetic field in the Ramsey region. This work was supported by the National Natural Science Foundation of China (No. 12004401) and Ministry of Science and Technology of China (No. 2013YQ09094304).

References

1. K. Gibble, S. Lea, and K. Szymaniec, in *2012 Conference on Precision Electromagnetic Measurements* (IEEE, 2012), p. 700.
2. J. Guéna, M. Abgrall, D. Rovera, P. Laurent, and S. Bize, "Progress in atomic fountains at LNE-SYRTE," IEEE Trans. Ultrason. Ferroelectr. Freq. Control **59**, 391 (2012).
3. T. P. Heavner, S. R. Jefferts, E. A. Donley, J. H. Shirley, and T. E. Parker, "NIST-F1: recent improvements and accuracy evaluations," Metrologia **42**, 411 (2005).
4. K. Szymaniec, S. E. Park, G. Marra, and G. W. Chalupczak, "First accuracy evaluation of the NPL-CsF2 primary frequency standard," Metrologia **47**, 363 (2010).
5. K. Szymaniec, W. Chalupczak, P. B. Whibberley, S. N. Lea, and D. Henderson, "Evaluation of the primary frequency standard NPL-CsF1," Metrologia **42**, 49 (2005).
6. Y. Ovchinnikov and G. Marra, "Accurate rubidium atomic fountain frequency standard," Metrologia **48**, 446 (2011).
7. R. Wynands and S. Weyers, "Atomic fountain clocks," Metrologia **42**, S64 (2005).
8. K. Szymaniec, S. N. Lea, K. Gibble, S. E. Park, K. Liu, and P. G. Owacki, "NPL Cs fountain frequency standards and the quest for the ultimate accuracy," J. Phys. Conf. Ser. **723**, 012003 (2016).
9. X. Wang, K. Liu, H. Cheng, W. Ren, J. Xiang, J. Ji, X. Peng, Z. Zhang, J. Zhao, M. Ye, L. Li, T. Li, B. Wang, Q. Qu, L. Liu, and D. Lü, "Optimization of temperature characteristics of a transportable ^{87}Rb atomic fountain clock," Chin. Opt. Lett. **17**, 080201 (2019).
10. S. Peil, J. L. Hanssen, T. B. Swanson, J. Taylor, and C. R. Ekstrom, "Evaluation of long term performance of continuously running atomic fountains," Physics **51**, 263 (2014).
11. R. Li, K. Gibble, and K. Szymaniec, "Improved accuracy of the NPL-CsF2 primary frequency standard: evaluation of distributed cavity phase and microwave lensing frequency shifts," Metrologia, **48**, 283 (2010).
12. V. Gerginov, N. Nemitz, S. Weyers, R. SChrDer, D. Griebsch, and R. Wynands, "Uncertainty evaluation of the caesium fountain clock PTB-CSF2," Metrologia **47**, 65 (2010).
13. J. Guéna, M. Abgrall, A. Clairon, and S. Bize, "Contributing to TAI with a secondary representation of the SI second," Metrologia **51**, 108 (2014).
14. S. R. Jefferts, J. Shirley, T. E. Parker, T. P. Heavner, and F. L. Walls, "Accuracy evaluation of NIST-F1," Metrologia **39**, 321 (2003).
15. Q. Wang, N. Zhang, R. Wei, S. Zhang, and Y. Wang, "Precision measurements of the ground-state hyperfine splitting of ^{85}Rb using an atomic fountain clock," Phys. Rev. A **100**, 022510 (2019).
16. S. H. Yang, K. J. Baek, T. Y. Kwon, Y. B. Kim, and H. S. Lee, "Second-order Zeeman frequency shift in the optically pumped cesium beam frequency standard with a dual servo system," Jpn. J. Appl. Phys. **38**, 6174 (2014).
17. X. Wang, J. Ruan, D. Liu, G. Yong, and S. G. Zhang, "The study of second-order Zeeman shift of the cesium fountain clock NTSC-F1," in *2016 IEEE International Frequency Control Symposium (IFCS)* (IEEE, 2016).
18. C. Y. Shi, R. Wei, Z. C. Zhou, D. S. Lü, T. Li, and Y. Z. Wang, "Magnetic field measurement on ^{87}Rb atomic fountain clock," Chin. Opt. Lett. **8**, 549 (2010).
19. Z. C. Zhou, R. Wei, C. Y. Shi, T. Li, and Y. Z. Wang, "Magnetic field measurement based on a stimulated two-photon Raman transition," Chin. Phys. B **20**, 247 (2011).
20. R. C. Dong, R. Wei, Y. B. Du, F. Zou, J. D. Lin, and Y. Z. Wang, "Magnetic field measurement by weak magnetic-sensitive Zeeman splitting," Appl. Phys. Lett. **106**, 152402 (2015).
21. R. Wei, Q. C. Ji, W. J. Zhao, and Y. Wang "Evaluation and suppression of the magnetic-induced Rabi broadening of magnetic-sensitive Ramsey fringes," J. Opt. Soc. Am. B **38**, 1078 (2021).
22. G. Breit and I. I. Rabi, "Measurement of nuclear spin," Phys. Rev. **38**, 2082 (1931).
23. E. Arimondo, M. Inguscio, and P. Violino, "Experimental determinations of the hyperfine structure in the alkali atoms," Rev. Mod. Phys. **49**, 31 (1977).